

# Author's Accepted Manuscript

Size distribution and shape properties of relatively small sea-ice floes in the Antarctic marginal ice zone in late winter

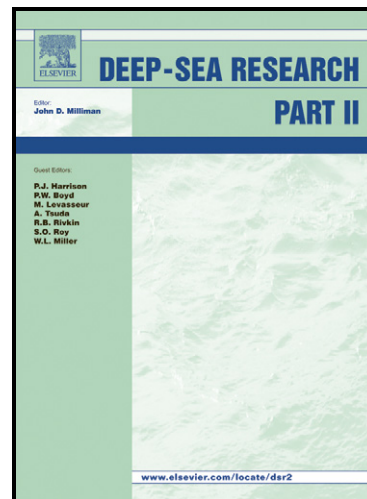
Takenobu Toyota, Christian Haas, Takeshi Tamura

PII: S0967-0645(10)00320-6  
DOI: doi:10.1016/j.dsr2.2010.10.034  
Reference: DSR II 2913

To appear in: *Deep-Sea Research II*

Cite this article as: Takenobu Toyota, Christian Haas and Takeshi Tamura, Size distribution and shape properties of relatively small sea-ice floes in the Antarctic marginal ice zone in late winter, *Deep-Sea Research II*, doi:[10.1016/j.dsr2.2010.10.034](https://doi.org/10.1016/j.dsr2.2010.10.034)

This is a PDF file of an unedited manuscript that has been accepted for publication. As a service to our customers we are providing this early version of the manuscript. The manuscript will undergo copyediting, typesetting, and review of the resulting galley proof before it is published in its final citable form. Please note that during the production process errors may be discovered which could affect the content, and all legal disclaimers that apply to the journal pertain.



[www.elsevier.com/locate/dsr2](http://www.elsevier.com/locate/dsr2)

**Title:**

**Size distribution and shape properties of relatively small sea-ice floes  
in the Antarctic marginal ice zone in late winter**

**Authors:**

**Takenobu Toyota<sup>1\*</sup>, Christian Haas<sup>2</sup>, and Takeshi Tamura<sup>3</sup>**

Submitted to Deep Sea Research II special volume on Antarctic sea ice

## Affiliation

1\*: Institute of Low Temperature Science, Hokkaido University

N19W8, Kita-ku, Sapporo, 060-0819, Japan (toyota@lowtem.hokudai.ac.jp)

\*corresponding author

Tel: +81-11-706-7431 Fax: +81-11-706-7142

2: Department of Earth & Atmospheric Sciences, University of Alberta

Edmonton, Alberta, T6G 2E3, Canada (Christian.Haas@ualberta.ca)

3: Institute of Low Temperature Science, Hokkaido University

N19W8, Kita-ku, Sapporo, 060-0819, Japan (tamutake@lowtem.hokudai.ac.jp)

**Abstract**

In the marginal sea ice zone (MIZ), where relatively small ice floes are dominant, the floe size distribution is an important parameter affecting melt processes given the larger cumulative perimeter of multiple small floes compared with a single ice floe of the same area. Smaller ice floes are therefore subject to increased lateral melt. However, the available data have been very limited so far. Analysis of sea ice in the Sea of Okhotsk revealed that while floe size distribution is basically scale invariant, a regime shift occurs at a size of about 40 m. In order to extend this preliminary result to the Antarctic MIZ and further examine the controlling factors, the first concurrent ice floe size and ice thickness measurements were conducted in the northwestern Weddell Sea and off Wilkes Land (around 64°S, 117°E) with a heli-borne digital video camera in the late winter of 2006 and 2007, respectively. The floe sizes ranged from 2 to 100 m. Our analysis shows: 1) the scale invariance and regime shift are confirmed in both regions; 2) the floe size at which regime shift occurs slightly increases from 20 to 40 m, with ice thickness, consistent with the theory of the flexural failure of sea ice; and 3) the aspect ratio is 1.6-1.9 on average, close to the previous results. Based on these results, the processes affecting the floe size distribution and the subsequent implications on melt processes are discussed. By applying a renormalization group method to interpret the scale invariance in floe size distribution, the fractal dimension is related to the fragility of sea ice. These results indicate the importance of wave-ice interaction in determining the floe size distribution.

Key words: Sea ice; Floe size distribution; Ocean-ice-atmosphere system; Ice melting;

Marginal ice zone; Scale invariance

Regional index term: Weddell Sea; East Antarctica

## 1. Introduction

The marginal sea-ice zone (MIZ), located between open ocean and the interior ice pack, is characterized by vigorous interaction with ocean waves. When ocean waves penetrate an ice cover, the wave energy is significantly attenuated by sea ice particularly for shorter wave periods, and in turn sea ice is fractured by the flexural force from penetrating waves (Squire and Moore, 1980; Wadhams et al., 1988; Squire et al., 1995). Thus relatively small ice floes, mostly less than 100 m in diameter, are dominant in the MIZ. As discussed by Steele et al. (1989), ice velocity significantly decreases for ice floes smaller than about 100 m due to the form drag effect. Additionally, Steele (1992) shows the melt rate of ice floes to significantly increase for floe sizes smaller than about 30 m because lateral melting becomes more important. Therefore, the floe size distribution is an important physical parameter in the MIZ to understand ice motion and melting. However, the available data have been very limited so far. Sea ice in the MIZ is subject to a complex interplay of thermodynamic and dynamic processes that affect the freeze and melt processes as well as the spread and retreat of the ice at a large scale. It is therefore critical to examine the general properties of floe size distribution in the MIZ and to include them in the numerical sea-ice models for climate prediction. At a small scale, floe size distribution can be used as a diagnostic tool of wave-ice interaction because it determines ocean wave activity and vice versa, as Lu et al. (2008) pointed out.

In the interior pack ice regions, the properties of sea-ice floe size distribution have been investigated by several researchers. For the Arctic and sub-polar regions, mainly ice floes larger than 100 m were analyzed with airborne radar, satellite images and aerial

photographs (e.g., Weeks et al., 1980; Rothrock and Thorndike, 1984; Matsushita, 1985; Holt and Martin, 2001; Toyota and Enomoto, 2002). Their results showed that the cumulative number distribution,  $N(d)$ , the number of floes per unit area with diameters no smaller than  $d$ , follows the power law, i.e.  $N(d) \propto d^{-\alpha}$ ,  $1.7 < \alpha < 2.9$ , indicating that floe size distribution is basically scale invariant. Yet at the same time these results raised the problem that the exponent  $\alpha$  often exceeds 2. Mathematically,  $\alpha$  corresponds to a fractal dimension, which describes the degree of complication of self-similar objects (Mandelbrot, 1967), and must be less than 2 for small ice floes, otherwise the ice area would be infinite (Rothrock and Thorndike, 1984). To solve this problem, Toyota et al. (2006) investigated the floe size distribution for floes ranging between 1 m and 1.5 km in diameter, by combining Landsat-7/ETM+ images and ship- and helicopter-borne video images in the southern Sea of Okhotsk. As a result, they found that a regime shift occurs at a size of 20-50 m and  $\alpha$  for smaller floes become reduced to 1.15. They hypothesized that the regime shift is induced by the effects of swell on floes of different sizes and thicknesses. Recently, Steer et al. (2008) and Lu et al. (2008) investigated the size distribution of ice floes smaller than 100 m with aerial photographs in the Antarctic during the melt season. In both cases changes in slope of  $N(d)$  were detected at a few tens of meters. While Lu et al. (2008) attributed it to the effect of upper truncation of a power law function (Burroughs and Tebbens, 2001), Steer et al. (2008) interpreted it as a change in the regime and estimated  $\alpha$  for smaller ice floes as about 1.9. This is significantly larger than the result of Toyota et al. (2006). Thus the knowledge of ice floes less than 100 m is still limited and the results obtained so far are variable depending on region and season. Due to a lack of ice thickness data, the mechanism for

the floe size distribution has been unknown. From theoretical studies based on a solution for wave propagation under floating elastic plates, it is shown that ice thickness is by far the most important factor for determining the scattering and break-up of ice (Meylan, 2002; Kohout and Meylan, 2008).

To improve the understanding of floe size distribution in the MIZ, concurrent floe size and ice thickness measurements were conducted for the first time with a heli-borne digital video camera in the Weddell Sea and off the Wilkes Land in late winter. These measurements covered floe sizes ranging from 2 m to 100 m. Ice thickness measurements were conducted using a heli-borne EM in the Weddell Sea and a video system off Wilkes Land. The major purpose of this study is to extend the preliminary result of the Okhotsk sea ice to the Antarctic MIZ, determine the general properties of the size distribution for relatively small ice floes, and to examine the processes affecting the floe size distribution and the subsequent impacts on melt process. This will, in turn, inform the parameterization of these processes in numerical sea-ice models. In the analysis special attention is paid to the scale invariant property, and to interpret this a simple renormalization group method (Turcotte, 1992) is applied. Based on the results, some possible melting processes are proposed.

## **2. Measurements**

Floe size measurements were conducted in the northwestern Weddell Sea during the expedition of the Winter Weddell Outflow Study (WWOS) and off Wilkes Land during the expedition of the Sea Ice Physics and Ecosystem Experiment (SIPEX).

### **2.1 Weddell Sea**

The WWOS expedition was performed with the German icebreaker R/V “Polarstern” for the period from August 25 to October 29, 2006 in the northwestern part of the Weddell Sea. This corresponds to the outflow region of the Weddell Gyre (Fig.1). The expedition was an interdisciplinary project, including physical and chemical oceanography, sea-ice physics and chemistry, biology, and bathymetry. The details are described in Lemke (2009) and the ice concentration in the study region from AMSR-E is shown in Fig 2. During this expedition, floe size observations were conducted with a heli-borne digital video camera (SONY, DCR-TRV30) on September 19 (60.1°S 50.8°W), October 17 (60.4°S 43.8°W) and October 18 (60.5°S 42.1°W), when the ship was crossing the MIZ. The heli-tracks were selected in a direction normal to the ice edge as shown in Fig. 3. Pictures of the ice conditions in each region are also shown in Fig 4. These figures show that all the observation areas between the open water and interior ice pack contained small ice floes, which is typical of the MIZ. During the observations, the weather was clear and there was only a small amount of cloud.

A heli-borne video camera, installed on the step of the helicopter with a tripod, recorded the ice conditions along each flight track. During the flights, the position and altitude were recorded every 10 seconds with GPS (Garmin, GPSMAP76) with a nominal accuracy of <15 m. The helicopter flew at several fixed altitudes, ranging from 90 to 1125 m, where the higher altitude was set for large floes and the lower for smaller floes (Table 1). To determine the scale of each image, the ship’s hull was embedded into an image at each representative altitude. Small fluctuations in altitude were also taken into account when calculating the scale. After the observation, the video tapes were downloaded to a personal computer and then image files with 640×480 pixels were

created every minute at each altitude in JPEG format (Fig.4). The representative width and length of images estimated for each altitude are summarized in Table 1. From this table, the horizontal resolution is estimated to be 0.1 m at the lowest altitude and 1.2 m at the highest altitude. A total of 122 images covering a combined area of 15.8 km<sup>2</sup> were used for the analysis.

On September 19 and October 18 ice thickness measurements were conducted with a heli-borne electromagnetic (HEM) sounding device around the observing areas. The HEM is flown at approximately 20 m above the ice and measures the distance from the instrument to the ice-seawater interface (i.e., ice bottom) using two low-frequency (3.7 and 112 kHz) electromagnetic (EM) induction channels. The ice thickness can be obtained by subtracting the height of the device above the combined snow and ice surface, which is measured by a laser profiler, resulting in a total ice+snow thickness measurement about every 4 m. Further details of the HEM system are described by Haas et al. (2009). A total of 4431 thickness observations were obtained along a 20 km track on September 19, while 27,220 measurements were obtained along a 126 km track on October 18. Due to the measurement accuracy, thicknesses less than 0.1 m were excluded from analysis which also effectively removes open water area from the data set. Since these observations were performed as part of a general survey of ice thickness distribution in the Weddell Sea, the area of coverage did not overlap completely with that of floe size measurement. Here, the thickness data that were obtained near the regions of floe size measurements (north of 60.4°S on Sep.19 and north of 60.8°S on Oct.18, see Fig.3) were selected for analysis. Within these regions, the ice conditions were almost homogeneous.

## 2.2 Wilkes Land

The SIPEX expedition was performed with the Australian icebreaker R/V “Aurora Australis” off Wilkes Land for the period of September 4 to October 17, 2007 (Fig.1). This expedition was also an interdisciplinary project, including sea-ice physics and chemistry, deployment of ice drifting buoy arrays, physical oceanography, measurement of aerodynamic parameters, and biology. During this cruise, ice floe size observations were conducted in the MIZ on October 8 (63.9°S 116.8°E) with the same video camera and in a similar method to the WWOS expedition. The flight direction was selected normal to the ice edge, approximately in the meridional direction (Fig. 5 and Fig. 6). The trajectory was recorded with a GPS (Garmin, eTrex Vista Cx) every 10 seconds. Since the altitude data of this GPS were unstable at that time, the pressure gauge and thermometer data, recorded every 10 seconds on board the helicopter, were used to calculate the flight altitude by integrating the hydrostatic equation. Unfortunately cloud was encountered at low and middle altitudes, forcing the helicopter to vary its altitude between 250 and 780 m. After the cruise, the video images were processed in the same way as in the WWOS expedition. A total of 52 images covering a combined area of 2.7 km<sup>2</sup> were analyzed. The horizontal resolution is estimated as 0.2 to 0.8 m, depending on the altitude.

Around the study area, ice thickness measurements were conducted with a downward-looking video camera installed on the ship’s rail that continuously recorded the ice conditions along the ship’s hull. After the cruise, ice thickness was measured on the video images for each ice floe that broke and turned into a side-up position

alongside of the hull. The scale was determined by lowering a measuring stick onto the ice surface while the ship was stationary. The detail of this method is described by Toyota et al. (2004). The reading error is less than a few centimetres. In this way, ice thickness data were obtained, though limited to two separate regions because the ship navigated this area mainly at night (Fig.6). However, it should be noted that deformed ice, which is hard to turn, is beyond the measuring capability of this method, and this method reflects only the thickness of relatively level ice. A total of 792 ice thickness measurements along 32 km of ship track were analysed.

### 3. Image processing

The video analysis was basically the same for the two Antarctic expeditions, and used the image processing technique developed by Toyota et al. (2006). Each ice floe was extracted according to its brightness, and then its area ( $A$ ), perimeter ( $P$ ), position in the image, and maximum/ minimum caliper diameters ( $d_{\max}/d_{\min}$ ) were measured using PC software. In this study, floe size ( $d$ ) is evaluated as the diameter of a circle that has the same area as that of the floe:  $d = \sqrt{4A/\pi}$ . In past studies, various definitions have been used for floe size. For example, Rothrock and Thorndike (1984) and Lu et al. (2008) used mean caliper diameter ( $d_{mc}$ : the average of caliper diameters in all orientations), while Steer et al. (2008) defined floe size ( $d_s$ ) as the side of the square that has the same area as that of floe. We adopted our definition because of its simplicity in calculation. In general, it was proved that these definitions of floe size are highly correlated:  $d = 0.92d_{mc}$ ,  $d = 1.13d_s$  (Rothrock and Thorndike, 1984).

In this analysis, the key is to precisely determine the edge of individual ice floes.

The detail is described by Toyota et al. (2006) and can be summarised as follows:

- 1) the RGB color brightness of each pixel is converted into grey scale (4096 classes);
- 2) the image contrast is emphasized by replacing the highest (lowest) 3% of pixels with the grey scale value 4095 (0), and interpolating the remaining pixels linearly between these two levels;
- 3) the threshold value that separates ice floes from open water is determined statistically for each image based on the histogram of brightness (usually bimodal);
- 4) the threshold value is then used to extract individual ice floes;
- 5) manual corrections are made to determine the floe edges for ice floes where segmentation with the selected threshold did not work. At this step, the edge line is drawn so that each floe is principally convex and matches the visual floe pattern as much as possible.

To facilitate analysis and maintain accuracy on the PC screen, the image is magnified to 2-8 times the original size if necessary. Since ice floes are often closely in touch with each other, the calculated threshold did not work effectively, and shadows behind the ice ridges cause further complications as they are sometimes automatically distinguished as seawater. For these reasons the manual corrections at step 5 became a major task. To reduce subjectivity in the analysis, the result obtained was reexamined at least twice.

Excluded from the analysis were those floes, which:

- 1) are intersected by the boundary of the image;
- 2) have an area less than 30 pixels; and

3) have an aspect ratios ( $d_{max}/d_{min}$ ) exceeding 5.

According to Criterion (2), the lower limits of the floe size are estimated as 1 to 8 m for WWOS and as 2 to 5 m for SIPEX, depending on the width of the image. Criterion (3) is included because extremely distorted ice floes are unsuitable for the definition of floe size. The floes that were excluded by this criterion were only 0.25 % and 0.03 % of the total in WWOS and SIPEX, respectively, and thus had no substantial effect on the results. One example which demonstrates the above analytical process is shown in Fig. 8. Consequently, the total number of ice floes analyzed from video amount to 27,490 for WWOS and 18,292 for SIPEX.

## 4. Results

### 4-1. Floe size distribution

Following past studies (e.g. Rothrock and Thorndike, 1984), the floe size distribution was expressed as the cumulative number distribution  $N(d)$ , defined by the number of floes per unit area with size no smaller than  $d$ . The results are shown in Fig. 9a for WWOS, where  $N(d)$  obtained individually at each altitude are drawn all together, and in Fig. 9b for SIPEX, where the results are integrated to a single  $N(d)$  value because there is no representative altitude. In both cases, the graphs are drawn only for the range where  $d$  is larger than the lower limit and  $N(d) > 5$ . It is found in both figures that while  $N(d)$  basically behaves like  $d^{-\alpha}$ , and hence floe size distribution is scale invariant, the exponent changes at a transition zone of about 20 to 40 m. The exponent  $\alpha$  for the smaller floe regime (hereafter, referred to as  $R_S$ ) is estimated by the least square method to be  $1.19 \pm 0.10$  for WWOS and  $1.26 \pm 0.19$  for SIPEX, with a significance level of

95%. For the larger floe regime (hereafter, referred to as  $R_L$ ) it is estimated to be  $5.00 \pm 0.90$  for WWOS and  $3.40 \pm 0.35$  for SIPEX. The results are summarized in Table 2, including the past result obtained from the Sea of Okhotsk. In Table 2, the approximate distance from ice edge ( $X$ ), and mean ice thickness and standard deviation are also shown. For ice floes off Wilkes Land, where ice conditions changed significantly with  $X$  (as shown in Fig. 7), the observation line was further divided into three sections (Fig. 6). The properties for each section are shown in Fig. 9c and summarized in Table 2.

The characteristics are summarized as follows:

- 1) in all regions there are two regimes of floe size within the size range of 2 to 100 m;
- 2) for  $R_S$ ,  $\alpha$  is much less than 2 with relatively small variation, while for  $R_L$  it exceeds 3 with large variation, depending on region;
- 3) the representative diameter ( $d_t$ ) of the transition zone between the two regimes slightly increases as the mean thickness ( $h_t$ ) of floes increases.

Points 1 and 2 are particularly important because these results solve the “infinite area” problem mentioned before and confirm the presence of two floe size regimes in the Antarctic MIZ, as proposed by Toyota et al. (2006). As described by Lu et al. (2008), there is a possibility that there is only one regime affected by upper truncation. In that case, the slope should become gradually steeper with  $d$ . When we look at the clear change in slope and the almost constant slope for  $R_L$ , however, it seems to be more natural to regard it as a different regime from  $R_S$ . Point 2 suggests there is a difference in a formation process of floe size distribution between  $R_L$  and  $R_S$ , which will be

discussed in the next section. It is interesting to note in Table 2 that the values of  $\alpha$  for  $R_S$  decrease as distance from the ice edge increases, suggesting that the activities of ocean waves are related to  $\alpha$ . Point 3 can be seen from the fact that  $d_t$ , which is about 30 m on Sep. 19 ( $h_i=1.08 \pm 1.07\text{m}$ ), increases to about 40 m on Oct.18 ( $h_i=1.63 \pm 1.19\text{m}$ ) in the Weddell Sea. For floes off Wilkes Land, as  $h_i$  increases towards the inner pack ice region (from  $0.46 \pm 0.15$  m at  $63.8^\circ\text{S}$  to  $0.66 \pm 0.40$  m at  $64.2^\circ\text{S}$ ),  $d_t$  gradually decreases (from 25 m at  $64.0^\circ\text{S}$  to 15 m at  $65.6^\circ\text{S}$ ). This result suggests that the regime shift is closely related to ice thickness. The detail will be discussed in the next section.

#### 4-2. Floe shape properties

The geometry of ice floes was also examined since the floe geometry may influence wave activity through the scattering process, as shown by Meylan (2002). Here, we use a parameter ( $d_p$ ), defined by the diameter of a circle which has the same perimeter as the floe:  $d_p=P/\pi$ , where  $P$  is the floe perimeter. When the ratio ( $R$ ) of  $d_p$  to  $d$  equals 1, the shape should be a perfect circle. The greater  $R$  becomes, the more distorted the shape becomes from a circle. Thus,  $R$  is regarded as a parameter of roundness. Fig. 10 shows the relationship between  $d$  and  $d_p$  for all ice floes analyzed. It is noticeable that they are surprisingly well correlated and  $R$  takes similar values, 1.14 to 1.22 for WWOS and 1.12 for SIPEX. These values are also close to the results obtained in the Beaufort Sea (1.11; Rothrock and Thorndike (1984)), in the Sea of Okhotsk (1.15; Toyota et al. (2006)) and in the Prydz Bay, Antarctica (1.13 to 1.22; Lu et al. (2008)). If we assume ice floes of elliptical shape, the values of 1.12, 1.14 and 1.22 for  $R$  correspond to

ellipses with aspect ratios of 2.30, 2.40, and 3.00, respectively. The reason why such a remarkable correlation between  $d$  and  $d_p$  can be found may be explained by the property of fractal objects, such that the ratio of  $(Perimeter)^{1/D}/(Area)^{1/2}$  is kept constant, where  $D$  is fractal dimension (Mandelbrot, 1982). Smirnov and Chmel (2006) applied this theory to drifting ice floes larger than several kilometers in the Arctic basin and also found a good correlation between area and perimeter. If this property is applied,  $d_p/d^D$  should be constant. From our analysis,  $D$  is estimated as 1.04 to 1.08, close to 1, which implies a good correlation between  $d$  and  $d_p$ . Yet a question still remains as to why their correlation is unchanged between the two regimes. This is for future work.

To examine the geometry more explicitly, the maximum and minimum caliper diameters,  $d_{max}$  and  $d_{min}$  respectively, are plotted for individual floes in Fig. 11. It is shown that they are also correlated, although not as well as  $d$  and  $d_p$ . The ratio  $d_{max}/d_{min}$  is estimated as  $1.91 \pm 0.58$  (Sep.19),  $1.80 \pm 0.52$  (Oct.17), and  $1.79 \pm 0.49$  (Oct.18) for WWOS and  $1.63 \pm 0.40$  for SIPEX. It is interesting that the value for SIPEX is somewhat smaller than those for WWOS and for the Okhotsk Sea ice ( $1.78 \pm 0.4$ ; Toyota et al., 2006), while somewhat larger than those for multi-year ice (1.5-1.6; Hudson, 1987). This can be explained by the higher wave activity off Wilkes Land compared with the other regions. According to the Antarctic climate model output presented by Connolley and Cattle (1994), the mean wind speed in winter is two to three times larger off Wilkes Land than in the Weddell Sea. Associated with this, the variation of sea level height which was derived from satellite altimetry (TOPEX/POSEIDON) is much higher off Wilkes Land than in the Weddell Sea and the Sea of Okhotsk (Chao and Fu, 1995). It is plausible that higher wave activity increase

the roundness of floes through collision processes though not so much as multi-year ice. However, it is noted that these values are somewhat smaller than the estimation from  $R$ . This is probably because ice floes usually do not have smooth outlines, associated with such processes as welding, breakup, and collisions, as will be discussed later.

To sum up the geometrical properties of ice floes, the aspect ratio is on average around 2, which means that floes are not of a circular shape but usually distorted. Interestingly, this value is unchanged between the two regimes and almost common in different regions except for multi-year ice. This suggests that the processes affecting floe geometry are relatively common, independent of sea-ice regions or floe size.

## **5. Discussion**

### **5-1. Ice regimes**

In the previous section, it was shown that there are two regimes in size distribution for ice floes ranging from 2 m to 100 m in diameter with the transition sizes  $d_t$  being at 20-40 m. Here we discuss what causes these regimes.

Concerning the response of sea ice to swell, theoretical studies have shown from the general equation of elastic motion that when ice floe size is smaller than 100 m, flexural failure becomes difficult for any period or amplitude of swell (Higashi et al., 1982; Fox and Squire, 1991; Meylan and Squire, 1994). Based on these theoretical results, Toyota et al. (2006) hypothesized that flexural failure by ocean swell is essential to produce a regime shift. In this study we would like to verify this idea by using ice thickness data. By investigating the behavior of ocean waves propagating normal to an infinite ice edge, Fox and Squire (1991) showed that the position of the strain magnitude peak relative to

the edge, corresponding to floe sizes produced due to break-up, increases significantly with the increase of ice thickness. The study therefore determined that a correlation exists between floe size and thickness. Here we examine the correlation quantitatively with the analytical solution of the dynamical properties of ice itself. According to the flexural theory of sea ice by Mellor (1986), the minimum ice length at which breakup will occur due to flexure stress is described as follows:

$$L_{\min} = \frac{\pi}{2} \cdot \left[ \frac{E \cdot h_i^3}{3k(1-\nu^2)} \right]^{1/4}$$

, where  $k$ ,  $E$ ,  $\nu$ , and  $h_i$  are the foundation modulus, Young's modulus, Poisson's ratio, and ice thickness, respectively. Thus if flexural failure is essential,  $d_t$  should be proportional to  $h_i^{3/4}$ , assuming that the other parameters are constant. According to the observational result in the Weddell Sea,  $d_t$  was estimated as about 30 m for  $h_i = 1.08$  m. And for the region where  $h_i = 1.63$  m,  $d_t$  was estimated as about 40 m, which almost coincides with the theoretically predicted value of 41 m ( $=30 \times (1.63/1.08)^{3/4}$ ). As for the floes off Wilkes Land, although direct comparison is not easy, it was shown that near the ice edge where  $h_i \approx 0.46$  m,  $d_t$  was estimated at about 20 m, while in the inner region where  $h_i \approx 0.66$  m,  $d_t$  was about 25 m which also nearly coincides with the predicted value of 26 m ( $=20 \times (0.66/0.46)^{3/4}$ ). Thus, our results support the hypothesis that  $d_t$  is basically determined by flexural failure. However, it should also be kept in mind that most of the models that examine the wave-ice interaction (e.g. Fox and Squire, 1991; Kohout and Meylan, 2008) assume one directional wave propagation into long ice plate. The effect of multi-directional waves and the floe geometry on the result needs to be clarified in the future.

## 5-2. Scale invariance

In section 4, it was shown that floe size distribution basically follows the power law within  $R_L$  and  $R_S$ , and the exponents  $\alpha$ , which define the fractal dimension, were obtained as a characteristic parameter. Here we discuss a formation process of floe size distribution based on the values of  $\alpha$ .

As for  $R_L$ ,  $\alpha$  exceeds 2 in all the cases. If only a fragmentation process occurs,  $\alpha$  should be less than 2 because the fractal dimension of the objects produced must not be greater than the Euclidean space dimension (two in this case) (Mandelbrot, 1982). Therefore, other processes such as welding should occur. It is often observed from the aircraft that several floes which are herding at different scales may consolidate to form a larger floe. Fig. 12 demonstrates such a situation. Smaller floes consolidate into bigger floes by rafting and more likely new ice growth. The size of herding is not unique, but has a wide range. Thus the herding and subsequent consolidation appears to work effectively and will therefore affect the size distribution for larger floes. Although the mechanism is not yet well understood, we infer that this process is associated with the interaction between ice floes and ocean swell and that the wavelength of swell plays an important role in determining the size of newly consolidated floes. The variable conditions of ocean swell, depending on region and time, would account for different values of  $\alpha$ . Therefore, ocean-sea ice interaction, in particular ocean swell, seems to be a key to the understanding of this process. However, it should be kept in mind that  $\alpha$  might be somewhat exaggerated due to a truncation effect resulting from underestimation of large floes in our method.

In contrast, a fracture/ fragmentation process seems to be dominant for  $R_S$  since  $\alpha$  is always less than 2. Scale invariance in fracture patterns of sea ice has been demonstrated over a wide range of sizes (e.g. Schulson and Hibler, 1991; Weiss, 2001). Therefore, to examine the formation process of size distribution, we apply a simple renormalization group (RG) method, which has been used successfully to explain the scale invariance in various phenomena through a physical fracture/ fragmentation process (Turcotte, 1992; Weiss, 2001). One merit of the RG method is that it allows us to treat the fragmentation process in two-dimensional space, which has not been achieved in the past wave-ice interaction models. In our analysis we introduce the concept of fragility, following Allegre et al. (1982) and Turcotte (1986) who used it as a physical parameter to explain the scale invariance in the mass distribution of rocks. Whereas Turcotte (1986) treated a 3D fragmentation of rocks, we consider a 2D fragmentation of ice floes. The fragility ( $f$ ) represents the probability of fragmentation of floes and is considered to be a function of the strength of sea ice and the intensity of ocean waves. Thus the purpose of the RG method is to provide a physical meaning of  $\alpha$  by relating  $f$  with  $\alpha$  in two-dimensional space.

Here we suppose that  $N_0$  rectangular ice floes with a length of  $d$  are initially present ( $0^{\text{th}}$  order cell) and fragment into smaller floes step by step. The basic hypothesis of this method is the assumption that at each step a cell fragments into four identical elements with the probability  $f$  ( $0 < f < 1$ ) which is constant at all scales (Fig. 13). For example, at the first step  $N_1$  fragments ( $1^{\text{st}}$  order cell) with a length of  $d/2$  are produced.  $N_1$  is calculated as  $4f \cdot N_0$ , while the number ( $N_0 a$ ) of remaining floes with a length of  $d$  ( $0^{\text{th}}$  order cell) is  $(1-f) \cdot N_0$ . At the second step, these fragments in turn produce  $N_2 (=4f \cdot N_1)$

fragments with a length of  $d/4$  ( $2^{\text{nd}}$  order cell), while the number ( $N_{1a}$ ) of  $1^{\text{st}}$  order cell is reduced to  $(1-f) \cdot N_1$  ( $= 4f(1-f) \cdot N_0 = 4f \cdot N_{0a}$ ). When this procedure is repeated, the number ( $N_{m a}$ ) of remaining  $m$ -th order cell with a length of  $d_m$  ( $= d/2^m$ ) can be expressed as follows:

$$\begin{aligned} N_{m a} &= (1-f) N_{m-1 a} = 4f(1-f) N_{m-1} \\ &= (1-f) (4f)^m N_0 \end{aligned}$$

Therefore, the cumulative number of  $m$ -th cells with a length greater than  $d_m$  is

$$N_{c,m} = (1-f)N_0 \sum_{k=0}^m (4f)^k = (1-f)N_0 \cdot \frac{(4f)^{m+1} - 1}{4f - 1} \quad (1)$$

Similarly, the cumulative number of  $(m+1)$ -th cells is

$$N_{c,m+1} = (1-f)N_0 \sum_{k=0}^{m+1} (4f)^k = (1-f)N_0 \cdot \frac{(4f)^{m+2} - 1}{4f - 1} \quad (2)$$

On the other hand, from the fractal property that the cumulative number  $N_c(r)$  behaves like  $r^{-\alpha}$ , we can describe

$$\frac{N_{c,m+1}}{N_{c,m}} = \frac{(d \cdot 2^{-(m+1)})^{-\alpha}}{(d \cdot 2^{-m})^{-\alpha}} = 2^\alpha \quad (3)$$

Combining (1), (2), and (3) with the assumption that  $4f > 1$  and  $m \gg 1$ , the following equation can be derived with a good approximation:

$$\alpha = \ln(4f) / \ln 2 \quad \text{or} \quad f = \frac{1}{2^{2-\alpha}} \quad (0 < \alpha < 2). \quad (4)$$

In the above calculation we assumed that a cell is fragmented into half-scaled elements at one step. Even if we assume  $1/3$ -scaled fragmentation occurs, the above discussion holds except  $\alpha = \ln(9f) / \ln 3$ . In general,  $\alpha = \ln(k^2 f) / \ln k$  is obtained for  $1/k$ -scaled

fragmentation. Since the general properties are similar for any value of  $k$ , here  $k=2$  is selected for simplicity.

The  $f$  values calculated from equation (4) for all regions are listed in Table 2. It is shown that  $f$  takes nearly 0.6 at 80-100 km from the ice edge, irrespective of the region, while  $f$  is reduced to 0.5 going into inner regions. This indicates that  $f$  is related closely to wave activity, and is consistent with the past observational results of wave energy attenuation (Squire and Moore, 1980; Wadhams et al., 1988). The possible scenario is as follows: first, ocean waves enter an ice cover with high intensity, and ice floes are fragmented into smaller floes. Then the ocean wave propagates further into the ice area with attenuated intensity. Thus in the inner region, ice floes are less fragmented with smaller  $f$ . This can be seen in Fig. 7, where floe size becomes larger in the interior region. The similar properties were also reported in the east Antarctic sea-ice zone by Lytle et al. (1997), where floe sizes increased from about 4 m near the ice edge to about 100 m in the interior region.

In this scenario, it is plausible that ice strength can be an important factor for  $f$  in the melting season when sea ice is significantly weakened due to melting. In this case,  $f$  is expected to increase significantly. This is supported by the result of Steer et al. (2008), who estimated  $\alpha$  to be as high as 1.9, corresponding to  $f=0.93$ , in the melting season. Such a high value of  $f$  indicates that sea ice is weak enough to be easily broken for any wave perturbations. Steer et al. (2008) concluded that a major process was the “relaxing” of ridges into small floes which was caused by divergent motion of pack ice. Although this may be true, we consider that some additional systematic break-up process should work to explain the scale invariant property in size distribution.

Therefore, the above discussion might be applicable to their result to some extent.

The decreasing trend of  $f$  and hence  $\alpha$  towards the inner region agree well with the past observational results (Kergomard, 1989; Lu et al., 2008). Kergomard (1989) showed that  $\alpha$  decreased from 1.8 within marginal zones to 1.0 within internal zones for ice floes northwest of Svalbard islands, close to our result. Lu et al. (2008) showed that  $\alpha$  decreased from 1.4 in the MIZ to 0.6 within internal zones for ice floes in the Antarctic Prydz Bay by fitting their results to the upper truncated power law,  $N(>L)/N_0 = C_0 (L^{-\alpha} - L_r^{-\alpha})$ . However, it is noted that despite the measurement in summer, Lu et al. (2008) estimated  $\alpha$  to be significantly lower than that of Steer et al. (2008), and even somewhat lower than our result. This is probably due partly to the different method and partly to the geographical conditions in Prydz Bay, which may provide some shelter from ocean waves and swell.

Finally, we would like to mention the effect of ice concentration. In high concentration ice fields, a non-linear transfer of wave energy may affect the wave attenuation and hence the break-up process (Wadhams et al., 1988). In our case, in the Weddell Sea, AMSR data (Fig. 2) and the observed ice conditions (Fig. 4) show the ice concentration to be quite homogeneous, ranging between 70 – 90% with some open water between floes. Off Wilkes Land, while the AMSR-E derived ice concentration along the observation line is about 90% or more with little variation (Fig.5), the observed ice conditions (Fig.7) show that some open water is present between floes. Therefore, we consider that in both cases it is unlikely that ice concentration has a significant effect on our results.

To sum up, the consideration of physical processes by means of  $\alpha$  clearly shows

that wave-ice interaction works effectively to produce the scale invariance in floe size distribution, but in a different way between  $R_L$  and  $R_S$ . Whereas both fragmentation and herding seem to work effectively within  $R_L$ , fragmentation is dominant and the fragility of sea ice can be a useful parameter to explain the floe size distribution within  $R_S$ .

### 5-3. Melting process

Here we discuss how much influence the size distribution has on the lateral melting process. To examine this, we calculate the total perimeter of ice floes belonging to two regimes ( $R_L$  and  $R_S$ ) and compare it with that of floes from a single regime ( $R_L$ ). Here let us suppose that the cumulative number distribution be described as:

Two regimes:  $N_a(d) = \beta_1 \cdot d^{-\alpha_1}$  for  $d_1 < d < d_2$  and  $N_b(d) = \beta_2 \cdot d^{-\alpha_2}$  for  $d > d_2$ ,

Single regime:  $N_b(d) = \beta_2 \cdot d^{-\alpha_2}$  for  $d > d_1$ .

Now we consider the floe size distribution where floe size ranges from  $d_1$  to  $d$ , and calculate the total perimeter as a function of  $d$ , which is expressed as

Two regimes:

$$\text{if } d_1 < d < d_2, P_{total}(d) = \int_{d_1}^d P(x) \cdot \left( -\frac{dN_a(x)}{dx} \right) \cdot dx$$

$$\text{if } d > d_2, P_{total}(d) = \int_{d_1}^{d_2} P(x) \cdot \left( -\frac{dN_a(x)}{dx} \right) \cdot dx + \int_{d_2}^d P(x) \cdot \left( -\frac{dN_b(x)}{dx} \right) \cdot dx$$

$$\text{Single regime: } P_{total}(d) = \int_{d_1}^d P(x) \cdot \left( -\frac{dN_b(x)}{dx} \right) \cdot dx$$

In calculation, ice concentration is assumed to be 0.8. Based on observational results, the values of 1 m, 30 m, 1.19, and 5.00 for WWOS and 1 m, 20 m, 1.26, and 3.40 for

SIPEX are assigned to  $d_1$ ,  $d_2$ ,  $\alpha_1$ , and  $\alpha_2$  respectively.  $P(x)$  is a perimeter of floe size  $x$  m, and given by  $\pi \cdot R \cdot x$ , where  $R$  is a roundness parameter,  $d_p/d$  ( $=1.12$ ).  $\beta_1$  and  $\beta_2$  are determined from the ice concentration and boundary conditions at  $d_2$ . In this way, the total perimeter was obtained for each case.

The result is drawn in Fig. 14, showing that the perimeter for floes with two regimes is as much as eight times less than that with a single regime. This indicates that the presence of  $R_S$  has a strong effect on the lateral melting process. Recently, the importance of lateral melting has been pointed out for Antarctic sea ice in the melting season (e.g. Nihashi et al., 2005). Therefore, accurate knowledge about floe size distribution, especially for floes smaller than a few tens of meters, will significantly improve our understanding of the melting processes of sea ice.

## 6. Conclusion

From the analysis of heli-borne digital video, the size distribution of ice floes over the 2 - 100 m range is evaluated in the MIZ of the Weddell Sea and off Wilkes Land in late winter. To examine the controlling factor of the size distribution, ice thickness data were obtained concurrently with heli-borne EM and video systems. It is revealed that in both regions there are two regimes for floes above and below a transition size ( $d_t$ ), which ranges from 20 to 40 m. The size distribution below  $d_t$  m was found to fit a power law,  $N(d) = \beta \cdot d^{-\alpha}$ , with an exponent  $\alpha$  ranging from 1.0 to 1.5, while above  $d_t$  m it also followed a power law but with a steeper slope,  $\alpha > 3$ . These results coincide with those of the Okhotsk sea ice (Toyota et al., 2006) and are suggested to be common properties in the general MIZ. The ice thickness observations which were first conducted together

with floe size distribution showed that  $d_i$  is approximately proportional to  $(h_i)^{3/4}$ , which is consistent with the theoretical prediction of flexural failure due to ocean wave propagation.

Based on the estimated  $\alpha$ , possible physical processes were discussed to interpret the scale invariance in the size distribution. As for  $R_L$ , since  $\alpha$  is always larger than 2, it is indicated that ocean waves and swell should work effectively not only on fragmentation but also on herding and subsequent consolidation of ice floes. As for  $R_S$ , by applying a simple RM method,  $\alpha$  was connected with the fragility of sea ice  $f$  as a physical parameter. As a result, it is shown that  $f$ , decreasing from 0.7 near the ice edge to 0.5 within the interior, is almost expressed as a function of the distance from ice edge, irrespective of the regions. This proves that wave intensity is a major factor in determining floe size distribution in late winter. On the other hand, in the melting season the fact that  $\alpha$  ( $f$ ) may be as high as 1.9 (0.93) within the internal region of the Weddell Sea (Steer et al., 2008) suggests that the weakness of sea ice due to melting is also a factor that enhances the fragmentation of ice floes. Thus wave activities and the seasonality of ice strength should be taken into account when explaining the floe size distribution.

The effect of floe size distribution on the lateral melting process is discussed by comparing the total perimeter of floes with two regimes ( $R_L$  and  $R_S$ ) with that of a single regime ( $R_L$ ). The calculation shows that it differs by as much as 8 times between these two cases, which indicates the importance of the presence of  $R_S$ .

The measurement of geometry for individual floes reveals that the aspect ratio ranges from 1.6 to 1.9 on average. The value is slightly larger in the Weddell Sea (1.79

to 1.91) than off Wilkes Land (1.63). This is probably attributed to the higher wave activity off Wilkes Land induced by stronger wind. It is likely that high wave activity increases the collision between floes resulting in floes with a rounder shape. Interestingly, there is little difference between the regimes of  $R_L$  and  $R_S$  in each region. This implies that the wave-ice interaction processes that determine floe geometry are relatively common, and independent of floe size.

Finally, we would like to discuss a possible role of the smallest end of  $R_S$  in the melting process. Our idea is as follows: suppose initially a certain floe size distribution is present in each regime. When some floes at the smallest end of  $R_S$  disappear, open water area is created, which enhances incoming ocean wave and induces breakup of floes within  $R_L$  and  $R_S$ . Then the ice floes become downsized on the whole and some of broken floes newly participate in the smallest end of  $R_S$ . Next some of these floes disappear again. As this procedure is repeated the average size of floes becomes smaller; however the size distribution is apparently kept constant except at the largest end. In this way, local equilibrium in the floe size distribution is attained. It is noteworthy that this process is analogous to Kolmogorov's theorem, which describes the local equilibrium state of the energy spectrum of turbulence as attained by the balance between the energy cascade originating from low wave number and the dissipation due to viscosity at large wave number (Kolmogorov, 1941). In this context, the smallest end of  $R_S$  plays the role of sea-ice loss due to melting at the small scale range, which is most important at the end phase. If this is true, it can be said that although our observation is just a snapshot, the floe size distribution obtained can be regarded as representative provided the wave activities are maintained. To prove this idea, the processes of melting

for small floes and breakup of large floes, along with the relevant time scales, must be examined in more detail.

In this study, size distribution is investigated for ice floes ranging from 2 m to 100 m in the Antarctic MIZ in late winter. Consequently, the relation of floe size distribution with wave-ice interaction and a melting process is revealed. This implies that wave-ice interaction is also important to the melting process, and to better understand this process further research into wave activities and ice properties is desirable.

### **Acknowledgments**

The authors deeply appreciate the support by all the crew and scientists of R/V “Polarstern” and R/V “Aurora Australis” during the expeditions of WWOS and SIPEX, respectively. Special thanks are given to the respective chief scientists, Prof. P. Lemke and Dr. A. Worby for their arrangements. Discussion with Prof. K. Golden, Dr. R. Massom and Prof. J. Ukita, proof reading by Dr. G. Williams, and valuable comments by anonymous reviewers were also helpful. Image processing was carried out using Image Pro Plus ver.4.0. This work was supported by JSPS KAKENHI 18510003 & 21510002 [Grant-in-Aid for Scientific Research (C)].

**References**

- Allegre, C.J., Le Mouel, J.L., Provost, A., 1982. Scaling rules in rock fracture and possible implications for earthquake prediction. *Nature* 297, 47-49.
- Chao, Y., Fu, L.-L., 1995. A comparison between the TOPEX/POSEIDON data and a global ocean general circulation model during 1992-1993. *Journal of Geophysical Research* 100 (C12), 24965-24976.
- Connolley, W.M., Cattle, H., 1994. The Antarctic climate of the UKMO unified model. *Antarctic Science* 6 (1), 115-122.
- Burroughs, S.M., Tebbens, S.F., 2001. Upper-truncated power laws in natural systems. *Pure Applied Geophysics* 158, 741-757.
- Fox, C., Squire, V.A., 1991. Strain in shore fast ice due to incoming ocean waves and swell. *Journal of Geophysical Research* 96 (C3), 4531-4547.
- Haas, C., Lobach, J., Hendricks, S., Rabenstein, L., Pfaffling, A., 2009. Helicopter-borne measurements of sea ice thickness using a small and lightweight digital EM system. *Journal of Applied Geophysics* 67, 234-241.
- Higashi, A., Goodman, D.J., Kawaguchi, S., Mae, S., 1982. The cause of the breakup of fast ice on March 18, 1980 near Syowa station, East Antarctica. *Proc. 4th Symposium on Polar Meteorology and Glaciology, National Institute of Polar Research, Tokyo, Japan*, pp. 222-231.
- Holt, B., Martin, S., 2001. The effect of a storm on the 1992 summer sea ice cover of the Beaufort, Chukchi, and East Siberian seas. *Journal of Geophysical Research* 106 (C1), 1017-1032.
- Hudson, R.D., 1987. Multiyear sea ice floe distribution in the Canadian Arctic Ocean.

- Journal of Geophysical Research 92(C13), 14,663-14,669.
- Japan Meteorological Agency, 2001. The statistical data of sea ice, Vol. 3, (Period: 1971-2000), Japan Meteorological Agency, Tokyo, Japan (CD-ROM).
- Kergomard, C., 1989. Analyse morphometrique de la zone marginale de la banquise polaire au nord-ouest du Spitsberg a partir de l'imagerie SPOT panchromatique. Bulletin de la Societe Francaise de Photogrammetrie et Teledetection, 115, 17-20.
- Kohout, A.L., Meylan, M.H., 2008. An elastic plate model for wave attenuation and ice floe breaking in the marginal ice zone. Journal of Geophysical Research 113, C09016, doi:10.1029/2007JC004434.
- Kolmogorov, A.N., 1941. The local structure of turbulence in incompressible viscous fluid for very large Reynolds numbers. Doklady Akademii Nauk SSSR 30, 301-305.
- Lemke, P., 2009. Reports on Polar and Marine Research Vol.586, The Expedition of the Research Vessel "Polarstern" to the Antarctic in 2006 (ANT-XXIII/7), with contributions of the participants, pp.145, Alfred-Wegener-Institute for Polar and Marine Research, Bremerhaven, Germany.
- Lu, P., Li, Z. J., Zhang, Z. H., Dong, X. L., 2008. Aerial observations of floe size distribution in the marginal ice zone of summer Prydz Bay. Journal of Geophysical Research 113, C02011, doi:10.1029/2006JC003965.
- Lytle, V.I., Massom, R., Worby, A.P., Allison, I., 1997. Floe sizes in the east Antarctic sea ice zone estimated using combined SAR and field data. Proc. 3<sup>rd</sup> European Remote Sensing Symp. on Space at the service of our Environment, Florence, Italy, pp. 931-936.

- Mandelbrot, B.B., 1967. How long is the coast of Britain? Statistical self-similarity and fractal dimension. *Science* 156, 636-638.
- Mandelbrot, B.B., 1982. *The Fractal Geometry of Nature*. Freeman, New York, USA.
- Matsushita, M., 1985. Fractal viewpoint of fracture and accretion. *Journal of the Physical Society of Japan* 54 (3), 857-860.
- Mellor, M., 1986. The mechanical behavior of sea ice. In: Untersteiner, N. (Eds.), *Geophysics of Sea Ice*, Springer, New York, USA, pp.165-281.
- Meylan, M.H., 2002. Wave response of an ice floe of arbitrary geometry. *Journal of Geophysical Research* 107(C1), 10.1029/2000JC000713.
- Meylan, M.H., Squire, V. A., 1994. The response of ice floes to ocean waves. *Journal of Geophysical Research* 99 (C1), 891-900.
- Nihashi, S., Ohshima, K.I., Jeffries, M.O., Kawamura, T., 2005. Sea-ice melting processes inferred from ice-upper ocean relationships in the Ross Sea, Antarctica. *Journal of Geophysical Research* 110, C02002, doi:10.1029/2003JC002235.
- Rothrock, D. A., Thorndike, A.S., 1984. Measuring the sea ice floe size distribution. *Journal of Geophysical Research* 89 (C4), 6477-6486.
- Schulson, E.M., Hibler, III, W.D., 1991. The fracture of ice on scales large and small: Arctic leads and wing cracks. *Journal of Glaciology* 37 (127), 319-322.
- Smirnov, V.N., Chmel, A.E., 2006. Self-similarity and self-organization of drifting ice cover in the Arctic basin. *Doklady Earth Science*, 411 (8), 1249-1252.
- Squire, V.A., Moore, S.C., 1980. Direct measurement of the attenuation of ocean waves by pack ice. *Nature* 283, 365-368.
- Squire, V.A., Dugan, J.P., Wadhams, P., Rottier, P.J., Liu, A.K., 1995. Of ocean waves

- and sea ice. *Annual Review of Fluid Mechanics* 27, 115-168.
- Steele, M., Morrison, J.H., Untersteiner, N., 1989. The partition of air-ice-ocean momentum exchange as a function of ice concentration, floe size, and draft. *Journal of Geophysical Research* 94(C9), 12739-12750.
- Steele, M., 1992. Sea ice melting and floe geometry in a simple ice-ocean model. *Journal of Geophysical Research* 97(C11), 17,729-17,738.
- Steer, A., Worby, A.P., Heil, P., 2008. Observed changes in sea-ice floe size distribution during early summer in the western Weddell Sea. *Deep-Sea Research Part II*, 55, 933-942.
- Toyota, T., Enomoto, H., 2002. Analysis of sea ice floes in the Sea of Okhotsk using ADEOS/AVNIR images. *Proc. 16<sup>th</sup> Int. Symposium on Ice, International Association for Hydro-Environment Engineering and Research, Dunedin, New Zealand*, pp. 211-217.
- Toyota, T., Kawamura, T., Ohshima, K.I., Shimoda, H., Wakatsuchi, M., 2004. Thickness distribution, texture and stratigraphy, and a simple probabilistic model for dynamical thickening of sea ice in the southern Sea of Okhotsk. *Journal of Geophysical Research* 109, C06001, doi: 10.1029/2003JC002090.
- Toyota, T., Takatsuji, S., Nakayama, M., 2006. Characteristics of sea ice floe size distribution in the seasonal ice zone. *Geophysical Research Letters* 33, L02616, doi:10.1029/2005GL024556.
- Turcotte, D.L., 1986. Fractals and fragmentation. *Journal of Geophysical Research* 91 (B2), 1921-1926.
- Turcotte, D.L., 1992. *Fractals and chaos in geology and geophysics*, Cambridge

- University Press, Cambridge, UK.
- Wadhams, P., Squire, V.A., Goodman, D.J., Cowan, A.M., Moore, S.C., 1988. The attenuation rates of ocean waves in the marginal ice zone. *Journal of Geophysical Research* 93 (C6), 6799-6818.
- Weeks, W.F., Tucker, W.B., Frank, M., Fungcharoen, S., 1980. Characteristics of surface roughness and floe geometry of sea ice over the continental shelves of the Beaufort and Chukchi Seas. In: Prichard, R.S. (Ed.), *Sea ice processes and models*, University of Washington Press, Seattle, USA, pp. 300-312.
- Weiss, J., 2001. Fracture and fragmentation of ice: a fractal analysis of scale invariance. *Engineering Fracture Mechanics* 68, 1975-2012.

**Figure captions**

Figure 1. Map showing cruise tracks and observation area for the WWOS and SIPEX expeditions with the ice edge on Sep. 30 (1971-2000) (JMA, 2001).

Figure 2. Ice concentration map by AMSR-E in the Weddell Sea, as of Oct. 17, 2006. The approximate areas of Fig. 3 are shown with thick black lines.

Figure 3. Helicopter (thick line) and ship (broken line) tracks in the Weddell Sea on: (a) Sep. 19, 2006; (b) Oct. 17, 2006; and (c) Oct. 18, 2006. Black circles denote the positions at which the images were used for analysis. Thick chained lines in (a) and (c) denote the region where ice thickness data obtained by heli-borne EM were used for analysis. W1, W2, and W3 are the areas with typical ice conditions on each date, and relate to the images in Fig.4.

Figure 4. Typical ice conditions at each section in the Weddell Sea. Refer to Fig. 3 for positions. The widths of the images are 376 m (W1), 565 m (W2), and 765 m (W3). Note that ice conditions are almost similar for each region.

Figure 5. Ice concentration map by AMSR-E off Wilkes Land as of Oct. 08, 2007. The area of Fig. 6 and the observation line are shown with thick black lines.

Figure 6. Heli (red line) and ship (blue line) tracks off Wilkes Land. Red circles denote the positions at which the images were used for analysis. Thick blue lines denote the

region where ice thickness data were obtained by video monitoring system. The observation lines are divided into three segments by black broken lines, according to the distance from the ice edge. S1, S2, and S3 are the areas with the typical ice conditions of each segment, and relate to the images in Fig. 7.

Figure 7. Typical ice conditions at each section off Wilkes Land. Refer to Fig. 6 for positions. The widths of the images are almost the same, 220 m (S1), 225 m (S2), and 226 m (S3). Note that floes become larger in the inner region.

Figure 8. One example, showing the process to extract ice floes from a video image. (a) Original video image; (b) the same as Fig. 8a but with each ice floe outlined in red after the process of determining ice edges; and (c) extracted floes to be measured.

Figure 9. Cumulative number distribution  $N(d)$  for (a) Weddell Sea, where green, red, blue lines denote the results on Sep. 19, Oct. 17, and Oct. 18, respectively; (b) off Wilkes Land, where all the data are included; and (c) off Wilkes Land, where the results are divided according to the distance from ice edge (refer to Fig.6 and Table 2). The numbers in Fig. 9c denote the transition size in meters.

Figure 10. Scatter plots between  $d$  and  $d_p$  for individual ice floes from video analysis. Broken lines show the regression obtained from the least square method. The slopes of the regression, corresponding to the roundness parameter  $R$ , are shown in Table 2. In the figure, c.c. means correlation coefficient. (a) Weddell Sea, on Sep. 19, 2006; (b)

Weddell Sea, on Oct. 17, 2006; (c) Weddell Sea, on Oct. 18, 2006; and (d) off Wilkes Land, on Oct. 08, 2007

Figure 11. Geometrical properties of ice floes obtained from video analysis. Scatter plot between  $d_{max}$  and  $d_{min}$  for (a) Weddell Sea, on Sep. 19, 2006; (b) Weddell Sea, on Oct. 17, 2006; (c) Weddell Sea, on Oct. 18, 2006; and (d) off Wilkes Land, on Oct. 08, 2007. Broken lines show the regression obtained from the least square method. The slopes of the regression, corresponding to the aspect ratio, are shown in Table 2.

Figure 12. Photograph of typical herding of ice floes in the Weddell Sea, taken from the helicopter at an altitude of 520 m on Sep. 19, 2006. The width of the photo is approximately 500 m. It is seen that various sizes of groups of floes are present.

Figure 13. Schematic picture illustrating a simple renormalization method for ice floes. At each step, a cell is fragmented into four elements with the probability  $f$ .

Figure 14. Total perimeter ( $P_{total}$ ) as a function of floe diameter ( $d$ ), assuming that floe sizes range from 1 m to  $d$  m with two regimes and single regime for (a) Weddell Sea and (b) off Wilkes Land

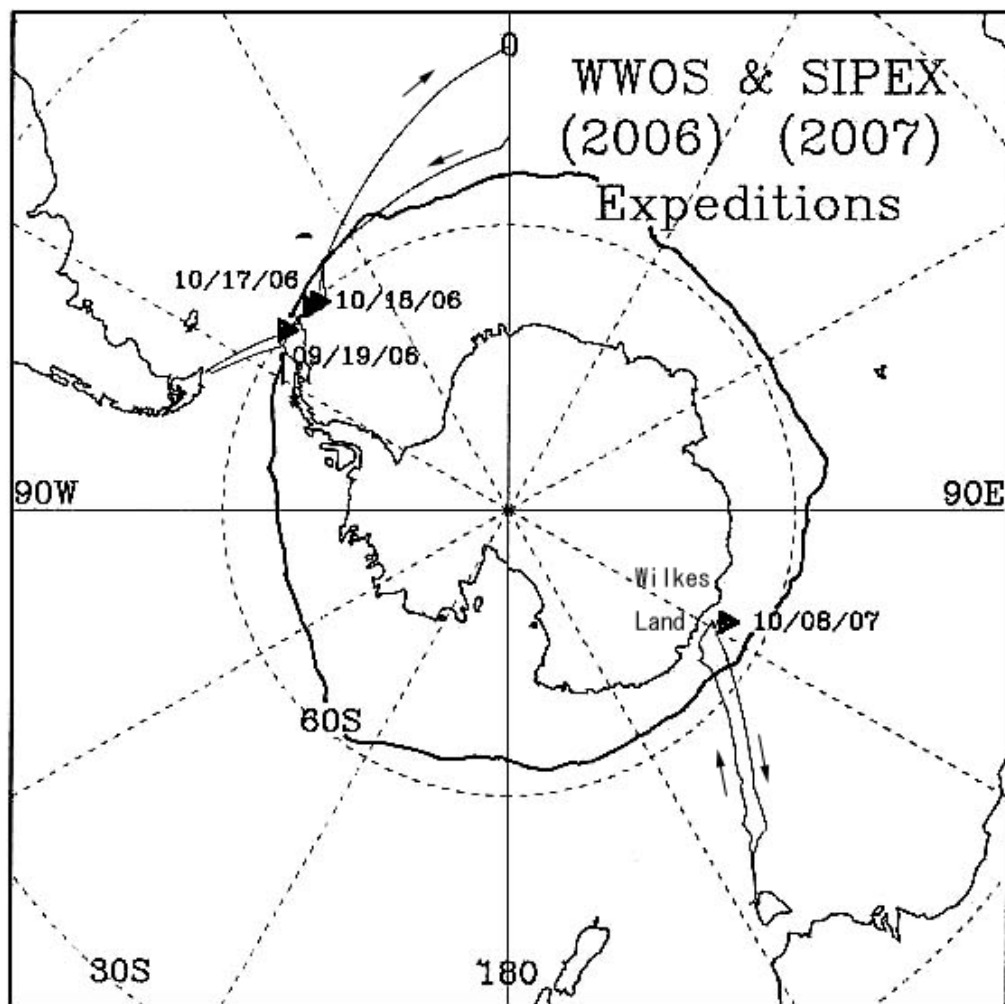


Figure 1. Geographical map of cruise tracks and observation area for the WWOS and SIPEX expeditions with the ice edge on Sep. 30 (1971-2000) (JMA, 2001).

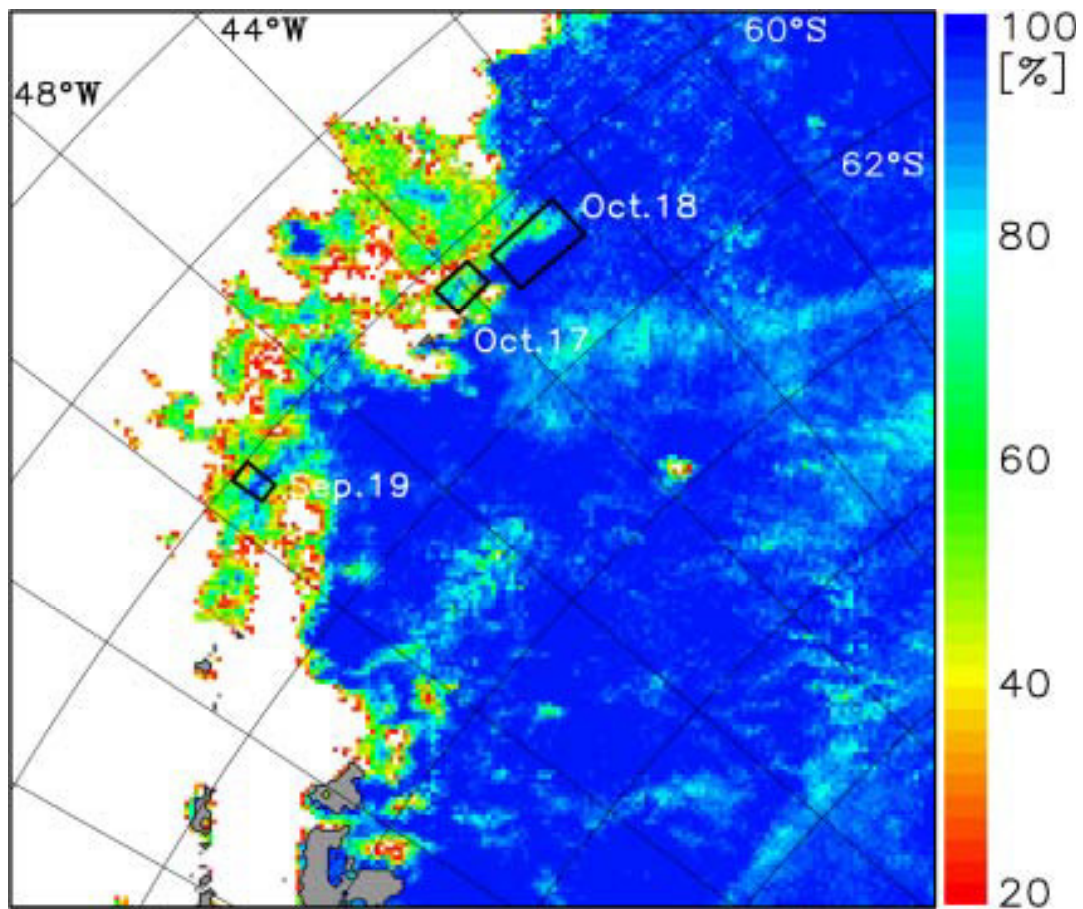


Figure 2. Ice concentration map by AMSR-E in the Weddell Sea, as of Oct. 17, 2006.  
The approximate areas of Fig.3 are shown with thick black lines.

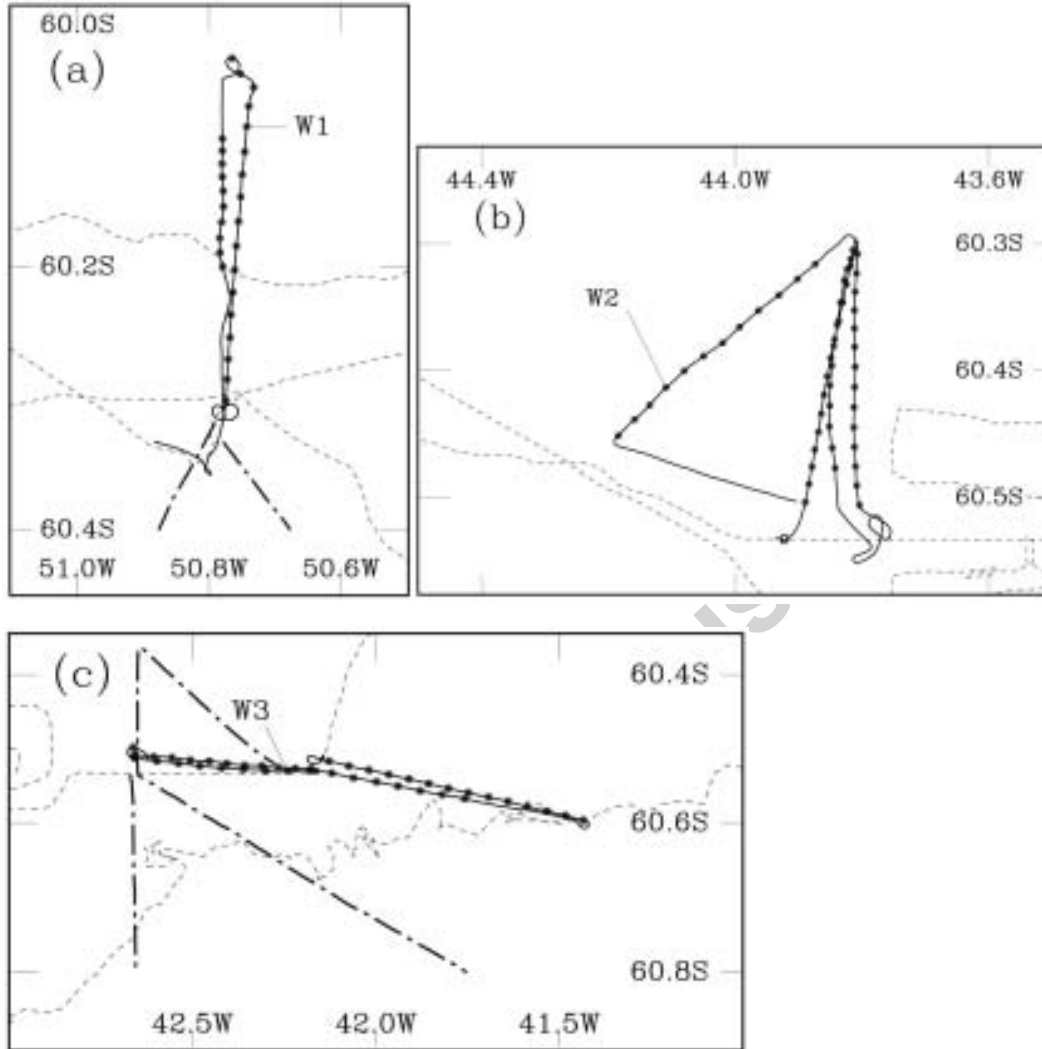


Figure 3. Heli (thick line) and ship (broken line) tracks in the Weddell Sea on:

(a) Sep. 19, 2006, (b) Oct. 17, 2006, and (c) Oct. 18, 2006.

Black circles denote the positions at which the images were used for analysis.

Thick chained lines denote the region where ice thickness data obtained by heli-borne EM were used for analysis. W1, W2, and W3 are the areas with typical ice conditions on each date, and relate to the images in Fig.4.

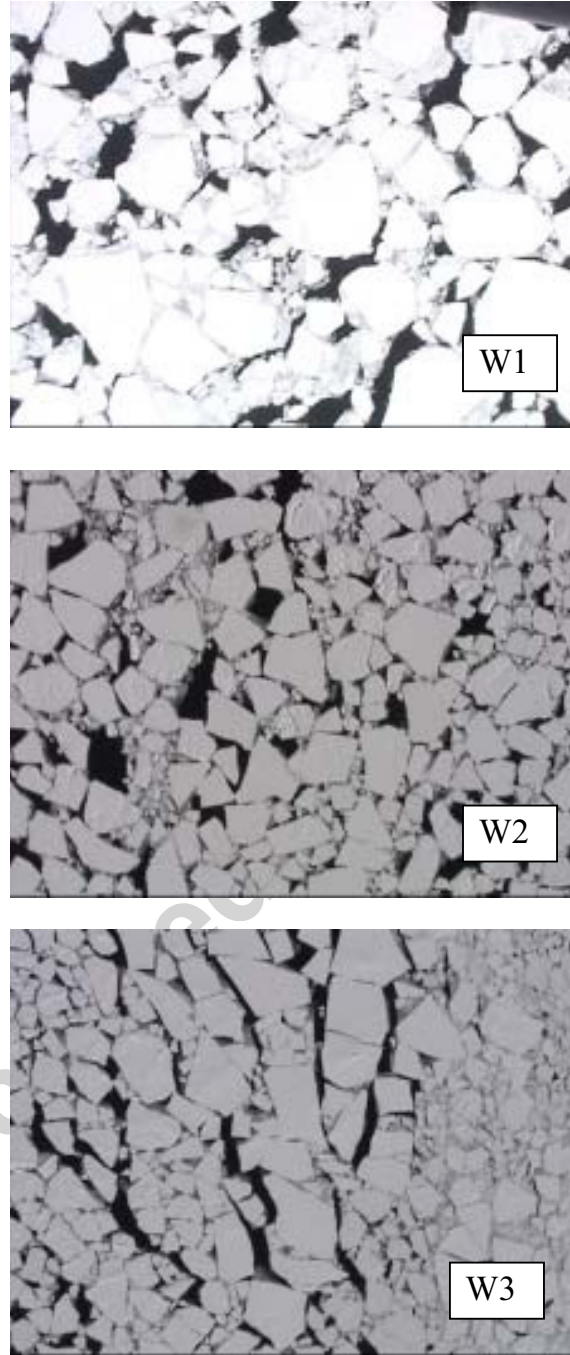


Figure 4. Typical ice conditions at each section in the Weddell Sea.

Refer to Fig.3 for positions.

The widths of the images are 376 m (W1), 565 m (W2), and 765 m (W3).

Note that ice conditions are almost similar for each region.

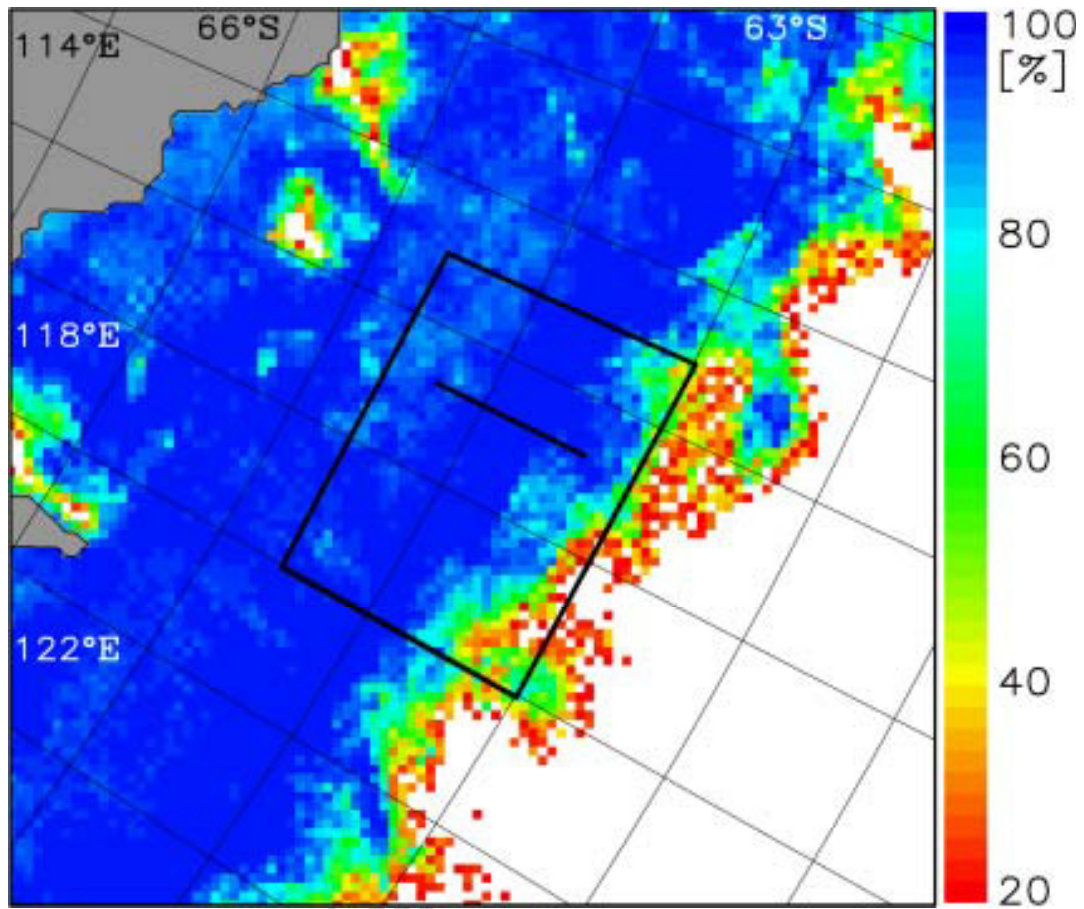


Figure 5. Ice concentration map by AMSR-E off Wilkes Land as of Oct. 08, 2007.

The area of Fig.6 and the observation line are shown with thick black lines.

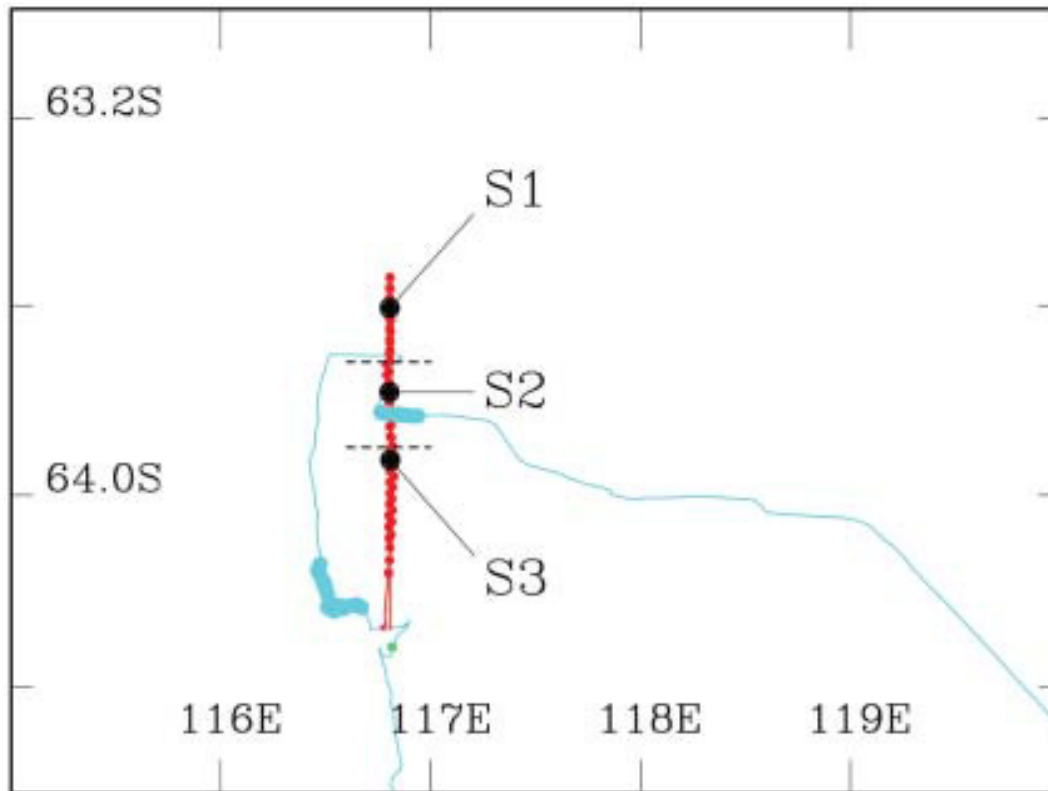


Figure 6. Heli (red line) and ship (blue line) tracks off Wilkes Land.

Red circles denote the positions at which the images were used for analysis. Thick blue lines denote the region where ice thickness data were obtained by video monitoring system. The observation lines are divided into three segments by black broken lines, according to the distance from the ice edge. S1, S2, and S3 are the areas with the typical ice conditions of each segment, and relate to the images in Fig.7.

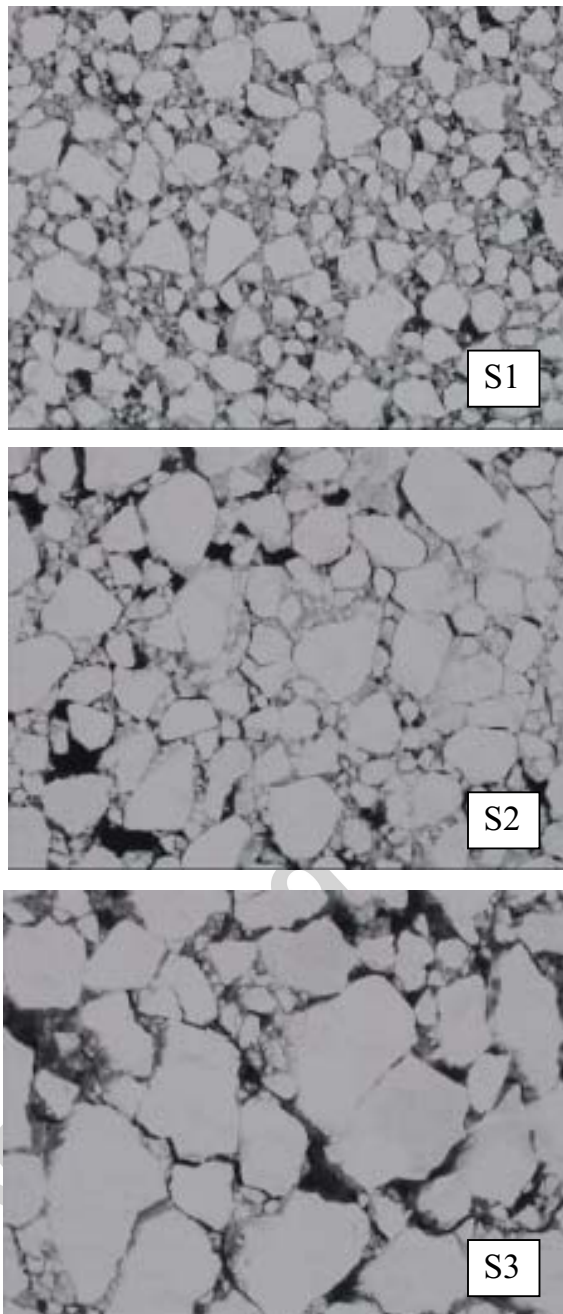


Figure 7. Typical ice conditions at each section off Wilkes Land.

Refer to Fig.6 for positions.

The widths of the images are almost the same, 226 m (S1), 225 m (S2), and 220 m (S3). Note that floes become larger in the inner region.

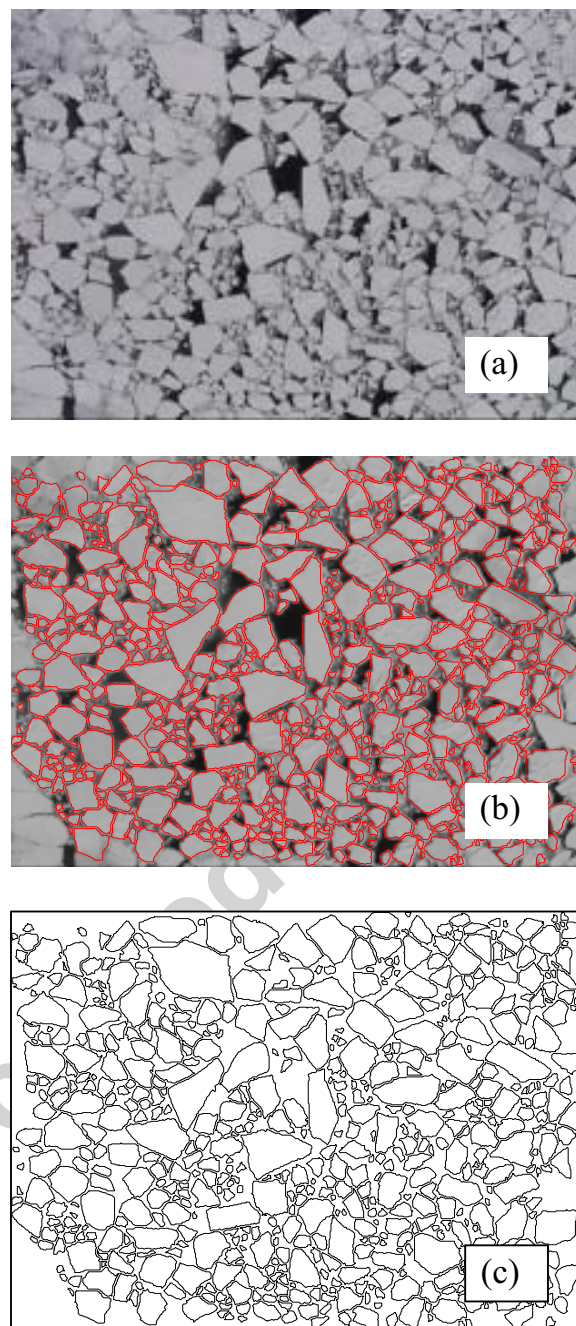


Figure 8. One example, showing the process to extract ice floes from a video image.  
(a) Original video image (b) The same as Fig.8a but each ice floe is outlined with a red line after the determining process of ice edges (c) Extracted floe to be measured.

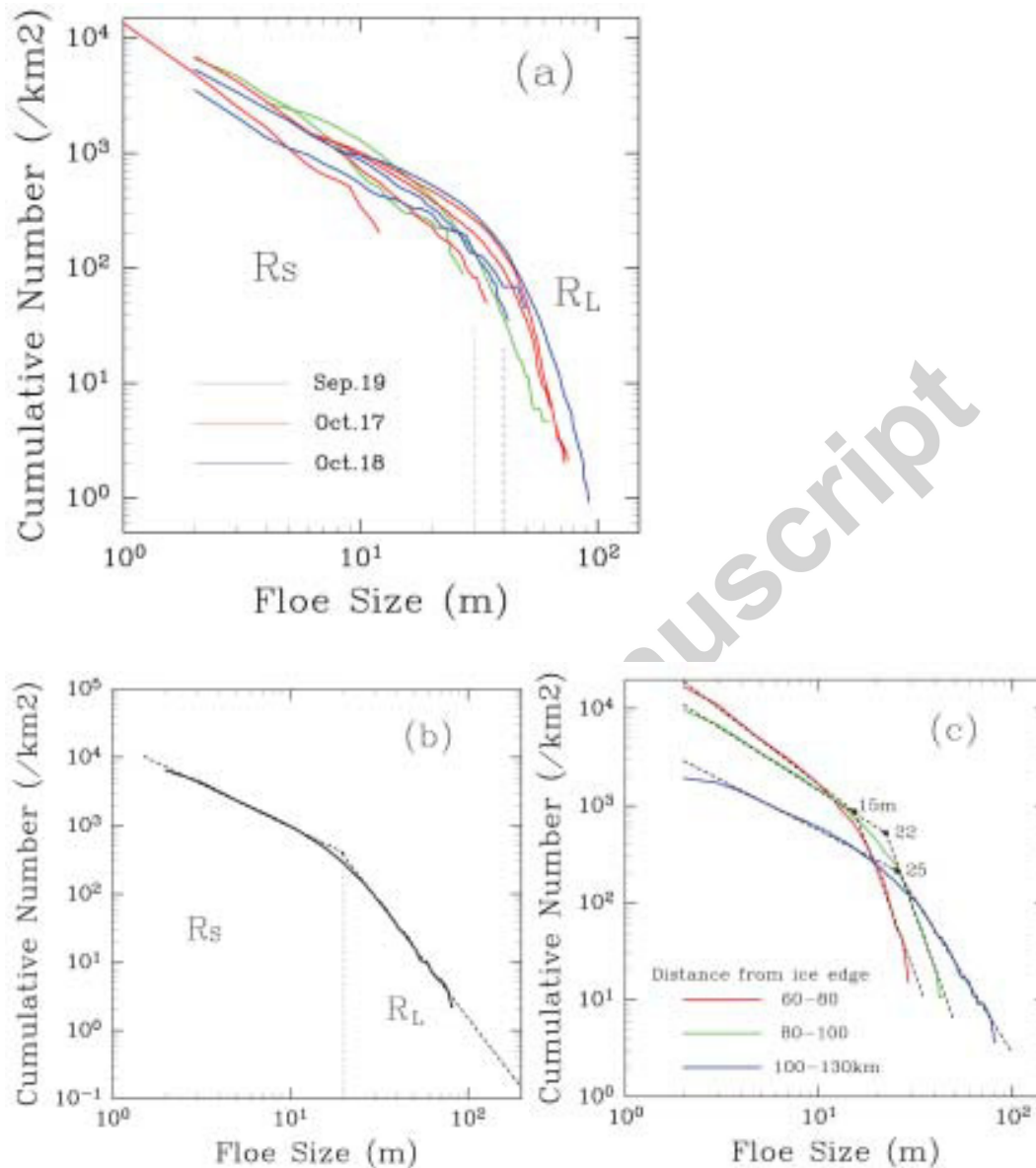


Figure 9. Cumulative number distribution  $N(d)$  for

(a) Weddell Sea, where green, red, blue lines denote the results on Sep. 19, Oct. 17, and Oct. 18, respectively, (b) off Wilkes Land, where all the data are Included, and (c) off Wilkes Land, where the results are divided according to the distance from ice edge (refer to Fig.6 and Table 2). The numbers in Fig.9c denote the transition size in meter.

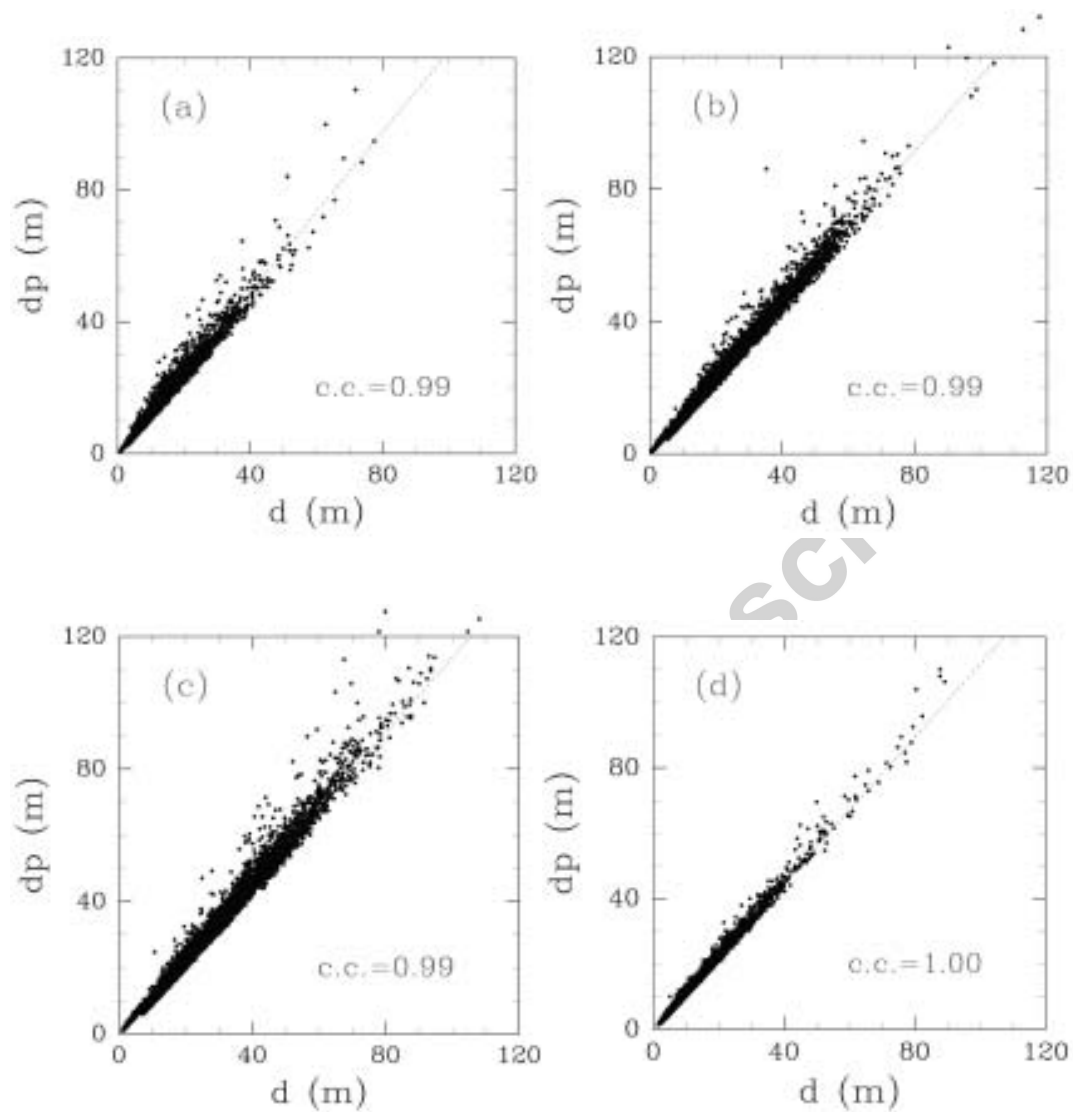


Figure 10. Scatter plots between  $d$  and  $d_p$  for individual ice floes from video analysis.

Broken lines show the regression obtained from the least square method.

The slopes of the regression, corresponding to the roundness parameter  $R$ , are shown in Table 2. In the figure, c.c. means correlation coefficient.

- (a) Weddell Sea, on Sep. 19, 2006    (b) Weddell Sea, on Oct. 17, 2006,  
 (b) Weddell Sea, on Oct. 18, 2006    (d) off Wilkes Land, on Oct. 08, 2007

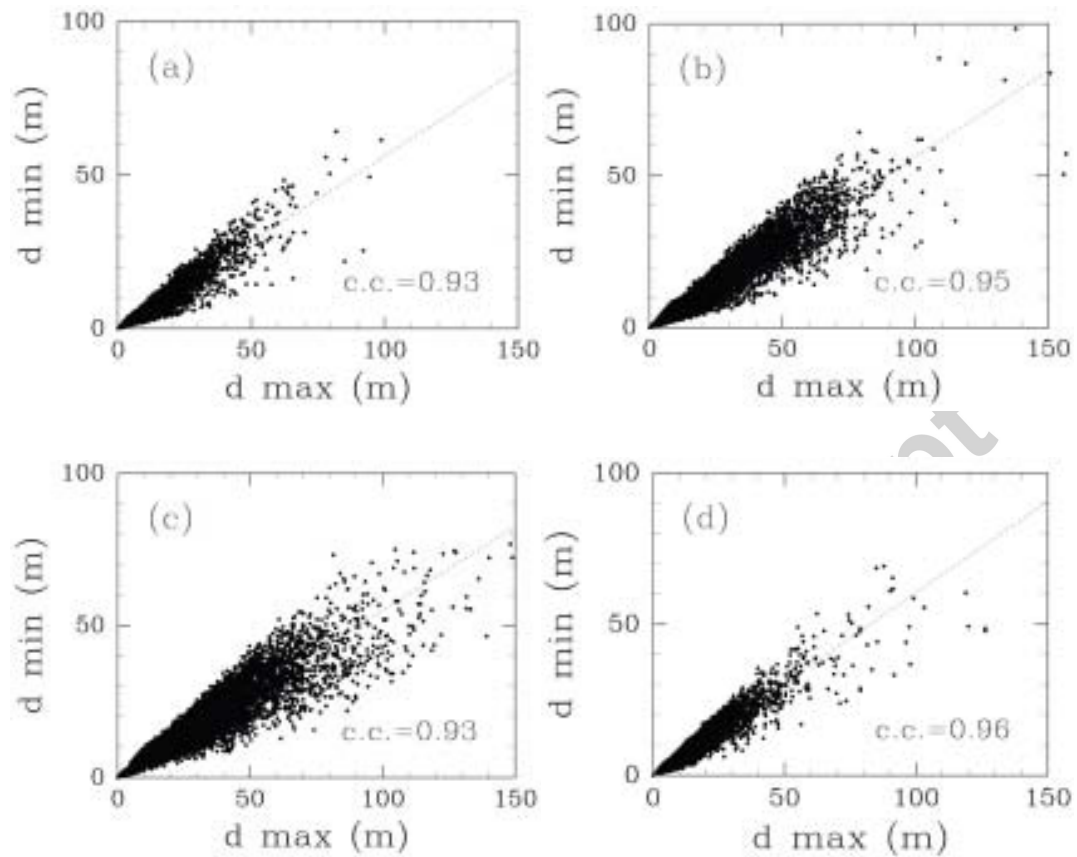


Figure 11. Geometrical properties of ice floes obtained from video analysis.

Scatter plot between  $d_{max}$  and  $d_{min}$  for (a) Weddell Sea, on Sep. 19, 2006  
 (b) Weddell Sea, on Oct. 17, 2006, (c) Weddell Sea, on Oct. 18, 2006,  
 and (d) off Wilkes Land, on Oct. 08, 2007.

Broken lines show the regression obtained from the least square method.

The slopes of the regression, corresponding to the aspect ratio, are shown in Table 2.



Figure 12. Photograph of typical herding of ice floes in the Weddell Sea, taken from the helicopter at an altitude of 520 m on Sep. 19, 2006. The width of the photo is approximately 500 m. It is seen that various sizes of groups of floes are present.

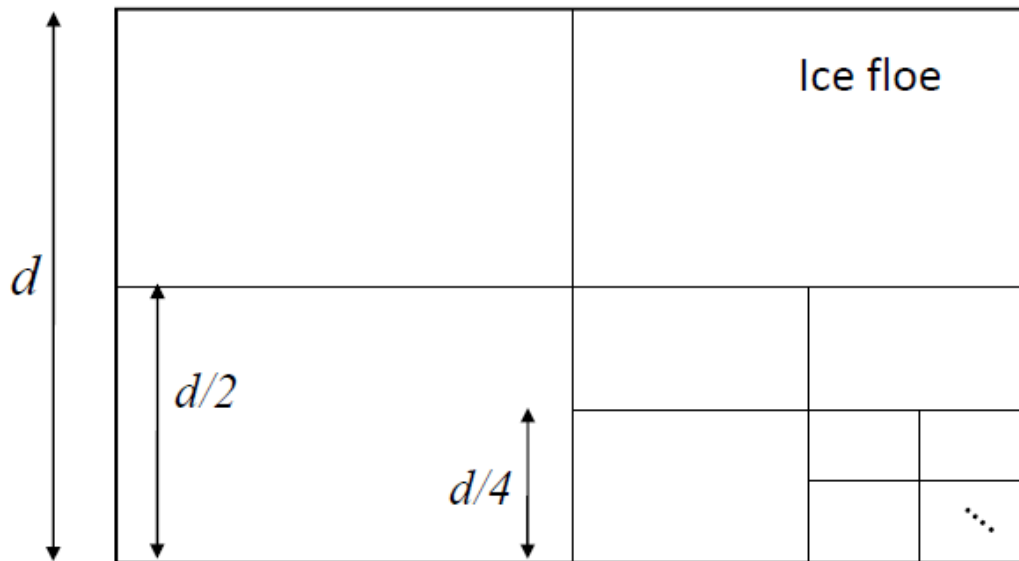


Figure 13. Schematic picture illustrating a simple renormalization method for ice floes.

At each step, a cell is fragmented into four elements with the probability  $f$ .

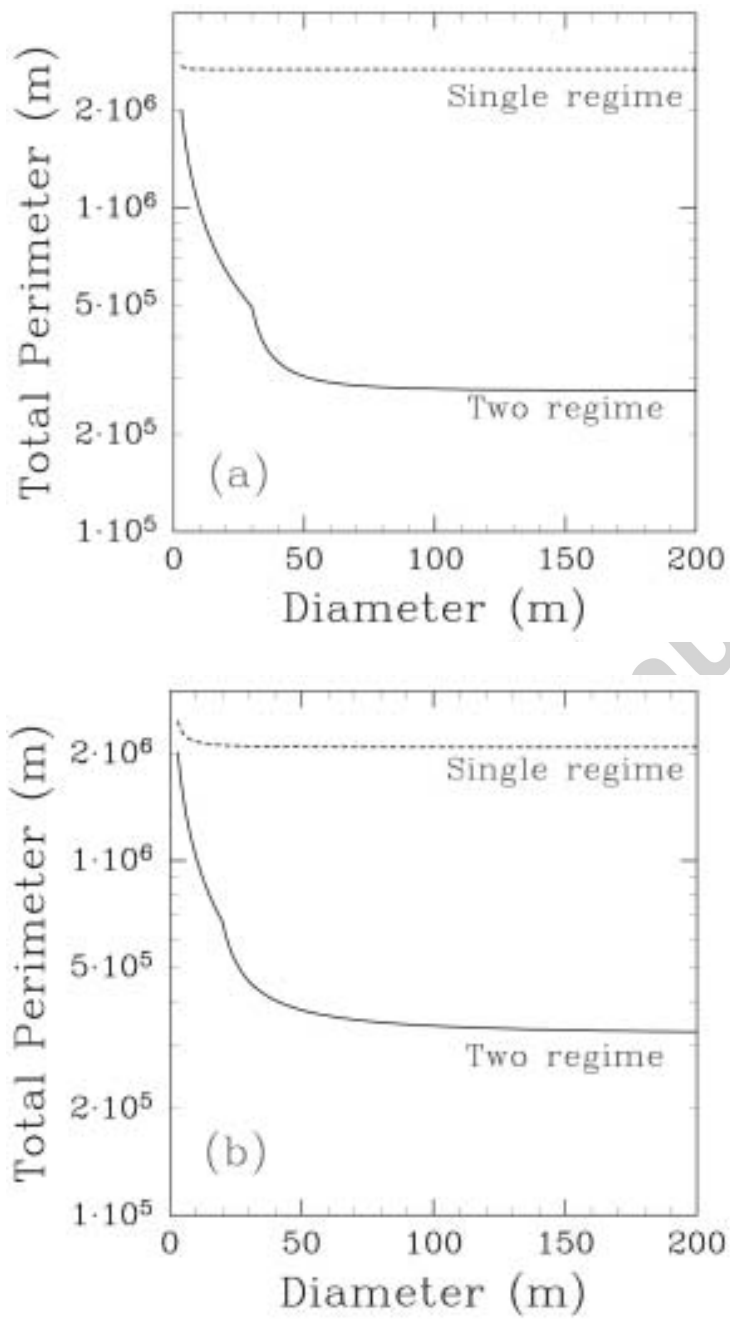


Figure 14. Total perimeter ( $P_{total}$ ) as a function of floe diameter ( $d$ ), assuming that floe sizes range from 1 m to  $d$  m with two regimes and single regime for (a) Weddell Sea and (b) Off Wilkes Land

**Table 1. General information on the measurements of ice floe size distribution from a helicopter during WWOS expedition in 2006.**

Date	File name	Mean Latitude (South)	Mean Longitude (West)	Mean altitude (m)	Number of video images	Mean size of each video image (m×m)	Total Area ( $\times 10^4 \text{m}^2$ )	Number of floes
09/19/06	0919a	-60.1496	-50.7807	125±8	10	71 × 95	6.7	724
	0919b	-60.1668	-50.7574	498±30	17	257 × 342	149.8	4382
10/17/06	1017a	-60.4115	-43.8557	90±9	14	39 × 53	2.9	748
	1017b	-60.3828	-43.8379	159±10	13	84 × 111	12.2	1598
	1017c	-60.4063	-43.8106	821±22	14	429 × 573	344.5	5390
	1017d	-60.3835	-44.0334	796±17	12	416 × 555	277.6	4461
10/18/06	1018a	-60.5192	-42.4102	186±9	11	94 × 126	13.1	697
	1018b	-60.5335	-42.2359	1125±34	17	577 × 769	754.7	8101
	1018c	-60.5567	-41.7769	174±15	14	103 × 137	19.8	1389
Total					122		15.84 km <sup>2</sup>	27490

Table 2. Statistics of ice floe properties

Region	Date	Distance from ice edge (km)	Ice thickness (m)	Transition size of regime shift $d_t$ (m)	Exponent $\alpha$		Fragility of sea ice $f$ ( $0 < f < 1$ )	Roundness $R$ ( $d_p/d$ )	Aspect ratio ( $d_{max}/d_{min}$ )
					$R_L$ ( $d > d_t$ )	$R_S$ ( $2 < d < d_t$ )			
Sea of Okhotsk	02/11/03	~120	$0.52 \pm 0.20$	40	1.87	1.15	0.56	1.15	1.78
Weddell Sea									
Total	Sep-Oct, 2006	60-150	-	30-40	5.00	1.19	0.57	1.17	1.83
60.1S	50.8W	09/19/06	$1.08 \pm 1.07$	~30	5.18	1.39	0.66	1.22	1.91
60.4S	43.8W	10/17/06	-	~40	7.59	1.20	0.57	1.14	1.80
60.5S	42.1W	10/18/06	$1.63 \pm 1.19$	~40	6.19	1.05	0.52	1.14	1.79
Off Wilkes Land									
Total	10/08/07	60-130	-	20	3.40	1.26	0.60	1.12	1.63
63.5<lat.<63.7S	10/08/07	60-80	-	15	5.38	1.52	0.72	1.08	1.59
63.7<lat.<63.9S	10/08/07	80-100	$0.46 \pm 0.15$	22	5.51	1.26	0.60	1.10	1.65
63.9<lat.<64.2S	10/08/07	100-130	$0.66 \pm 0.40$	25	3.15	1.03	0.51	1.14	1.70

(\*) In the column of Region, the central positions are listed for the Weddell Sea, while the longitudes off Wilkes Land are all about 116.8E. The data for the Sea of Okhotsk is cited from Toyota et al. (2006).

As for  $\alpha$  and  $f$ , see text for details. The distance from ice edge was estimated approximately from AMSR-E and ASAR images.

Due to measurement accuracy, thickness less than 0.1 m was excluded from analysis for Weddell Sea ice.